Journal of Materials Chemistry A

Understanding Activity Origin for Oxygen Reduction Reaction on Bi-Atom Catalysts by DFT Study and Machine-Learning

Journal:	*Journal of Materials Chemistry A*
Manuscript ID	TA-ART-08-2020-008004.R1
Article Type:	Paper
Date Submitted by the Author:	19-Oct-2020

Complete List of Authors:	Deng, Chaofang; Chongqing University of Education Su, Yang; Chongqing University Li, Fuhua; Chongqing University, School of Chemistry and Chemical Engineering Shen, Weifeng; Chongqing University, School of Chemistry and Chemical Engineering Chen, Zhongfang; University of Puerto Rico, Department of Chemistry Tang, Qing; Chongqing University, School of Chemistry and Chemical Engineering

Understanding Activity Origin for Oxygen Reduction Reaction on Bi-Atom Catalysts by DFT Study and Machine-Learning

Chaofang Deng[a,b], Yang Su[b], Fuhua Li[b], Weifeng Shen[b], Zhongfang Chen*, [c]and Qing Tang*,[b]

[a] Cooperative Innovation Center of Lipid Resources and Children's Daily Chemicals, Chongqing University of Education, Chongqing 400067, China

[b] School of Chemistry and Chemical Engineering, Chongqing Key Laboratory of Theoretical and Computational Chemistry, Chongqing University, Chongqing 401331, China

[c] Department of Chemistry, University of Puerto Rico, Rio Piedras, San Juan, PR 00931, USA

* To whom correspondence should be addressed. E-mail: zhongfangchen@gmail.com; qingtang@cqu.edu.cn.

Abstract: The bi-atom catalysts (BACs) have attracted increasing attention in important electrocatalytic reactions such as oxygen reduction reaction (ORR). Here, by means of density functional theory simulations coupled with machine-learning technology, we explored the structure-property correlation and catalytic activity origin of BACs, where metal dimers coordinated by N-doped graphene (NC). We first sampled 26 homonuclear (M_2/NC) BACs and constructed the activity volcano curve. Disappointedly, only one BAC, namely Co_2/NC, exhibits promising ORR activity, leaving a considerable room for enhancement in ORR performance. Then, we extended our study to 55 heteronuclear BACs (M_1M_2/NC) and found that 8 BACs possess competitive or superior ORR activity compared with the Pt(111) benchmark catalyst. Especially, CoNi/NC shows the most optimal activity with a very high limiting potential of 0.88 V. The linear scaling relationships among the adsorption free energy of *OOH, *O and *OH species are significantly weakened on BACs as compared to that on transition metal surface, indicating that it is difficult to precisely describe the catalytic activity with only one descriptor. Thus, we adopted machine-learning techniques to identify activity origin for ORR on BACs, which is mainly governed by simple geometry parameters. Our work not only identified the promising BACs yet unexplored in experiment, but also provides useful guidelines for the development of novel and highly efficient ORR catalysts.

Introduction

The proton exchange membrane fuel cell (PEMFC) is an attractive way to produce electrical energy from direct electrochemical conversion of oxygen and hydrogen.[1, 2] However, to make the PEMFC process economically attractive, there are many challenges to be conquered, and one of them is the slow kinetics of the oxygen reduction reaction (ORR) at the cathode.[3-5] The key to improve the sluggish ORR performance is to find a viable and highly active electrocatalyst.[6-10] Presently, Pt and its alloys remain the most common and efficient electrocatalysts,[11-14] yet the dilemma of their scarcity and poor durability put large obstacles on the widespread applications. These thus call for the development of more promising and cost-effective alternatives of ORR electrocatalysts.

In recent years, single-atom catalysts (SACs), where the active metal atoms are singly distributed on the support, have attracted tremendous research attention.[15-21] Despite significant advances made in SACs catalysts, their capabilities toward ORR are still unsatisfied, bringing a great challenge to develop newly efficient ORR electrocatalysts. Notably, recent experimental and theoretical studies showed that introducing the secondary metal atoms can modulate the electronic properties to further boost the activity of SACs, indicating the great prospect of bi-atom catalysts (BACs). [22-30] Experimentally, among others, Xiao *et al.* synthesized the binuclear Co_2N_5 active sites, which showed much higher ORR activity than the single CoN_4 active site.[23] Remarkably, Han *et al.* demonstrated that binary CoNi sites in nitrogen-doped hollow carbon nanocubes exhibit outstanding catalytic performance

for bifunctional oxygen reduction and evolution reactions.[24] Theoretically, Guo *et al.* showed that BACs can help conquer the activity and selectivity challenges of catalysts towards electrochemical nitrogen reduction,[27] and Li *et al.* demonstrated that the heteronuclear BAC, $Fe_1Cu_1@C_2N$, outperforms its homonuclear counterparts ($Fe_2@C_2N$ and $Cu_2@C_2N$)towards CO oxidation.[28] These studies indicate that not only the homo-nuclear but also the hetero-nuclear metal dimer can function as potential ORR electrocatalysts, and heteronuclear BACs may behave ever better. Despite these recent progresses, the development of BACs is still in its infancy. The underlying activity origin and possible structure-activity correlation of BACs still remain unclear. These urgent issues lay the foundation for the rational design of efficient BACs for ORR. Particularly, considering the large number of transition metals in the periodic table, the combinatorial possible homo- and hetero-bi-atom dimers are numerically very large, which yields grand experimental challenge to synthesize and characterize all potential combinations. To this end, theoretical calculations aided by data-mining techniques, such as machine-learning, is highly promising to fast screen the high-performance catalyst candidates and understand the origins behind the activity of BACs.

Note that the traditional SACs can be regarded as the smallest size limit of pure metals, while the BACs, the hetero-bi-metals, in particular, can be viewed as the size limit of hybrid alloy materials. To accelerate the discovery of prospective BACs, herein, systematic density functional theory (DFT) calculations were employed to explore the ORR activity of BACs. Taking the N-doped graphene (NC) as the

stabilizing substrate, we explored the ORR activity of metal dimers anchored on NC and sampled the large potential combinations space of both homonuclear (M_2/NC) and heteronuclear (M_1M_2/NC) BACs. We demonstrated that one homonuclear BAC and eight heteronuclear BACs can achieve remarkable activity improvement, which is comparable or even superior to the Pt-based catalysts. Among them, a noble metal-free BAC, namely CoNi/NC, shows the most optimal activity with a very high limiting potential of 0.88 V. Furthermore, combining machine-learning method, we identified the key factor that governs the ORR activity of BACs. The geometric distance between metal dimer and the coordinated N as well as the distance between the two metal centers are found to play the key role. This work not only identified highly promising BACs to replace the precious Pt catalysts, but also provided practical guidance for discovering and designing of high-performance catalysts.

Methods

Spin-polarized DFT calculations were performed by Vienna *ab initio* simulation package (VASP).[31] The electron exchange-correlation is represented by the functional of Perdew-Burke-Ernzerhof (PBE) with generalized gradient approximation (GGA).[32] The interaction between ion cores and valence electrons is described by the projector augmented wave (PAW) method.[33] A cutoff energy was set as of 400 eV and the Brillouin zone was sampled by 3 × 3 × 1 k-points. A vacuum space of 15 Å was adopted to minimize interactions between neighboring catalyst images. A dispersion correction using the DFT-D3 method was carried out to describe the van der Waals

(vdW) interactions between the reactants and the catalyst.[34] To simulate the H_2O solvent environment, the Poisson−Boltzmann implicit solvation model was employed with a dielectric constant of ε = 80 for water.[35, 36] The convergence threshold was set to be 1×10^{-5} eV for energy and 0.02 eV/Å for atomic force. To correct the magnetization, we considered different initial magnetic moments and smearing values. It is found that the initial magnetic moment plays little influence on the converged magnetic moments. However, the magnetic moments are sensitive to the smearing value. When a smearing width of 0.001 eV was adopted, the magnetic moment of metal dimer (Fe_2: $3\mu_B$, Co_2: $1\mu_B$, Ni_2: $0\mu_B$) is close to the results from previous report.[37] Thus, the smearing width was set as 0.001 eV for our DFT calculations. The catalyst was modeled by embedding a metal dimer center into a graphene lattice, where metal dimer coordinated with six nitrogen atoms. The rectangular lattice parameter of graphene is 17.22 Å × 17.04 Å and the geometry configuration is presented in Figure 1a.

The free energy change of each ORR elementary step (ΔG) was calculated based on the computational hydrogen electrode (CHE) model proposed by Nørskov and co-workers.[38, 39] In this model, the chemical potential of a proton/electron ($H^+ + e^-$) pair is equal to half of the gas-phase H_2 at standard hydrogen electrode (SHE) conditions. According to the CHE model, ΔG can be defined as equation (1),

$$\Delta G = \Delta E + \Delta ZPE - T\Delta S + \Delta G_{pH} + \Delta G_U \quad (1)$$

where ΔE is the total energy change directly obtained from DFT calculations. ΔZPE and ΔS are the difference of zero-point energy and entropy, respectively. T is the

temperature of 298.15 K. ΔG_{pH} and ΔG_U are caused by variations of the H^+ concentration and the electrode potential, respectively. Here the value of ΔG_{pH} is set as zero at acid conditions. For the free H_2 and H_2O molecules, the entropies were obtained from the NIST database. $S^0_{H_2}$ and $S^0_{H_2O}$ was the entropy under standard conditions obtained from the NIST database ($S^0_{H_2} = 130.68$ J/mol * K and $S^0_{H_20} = 188.84$ J/mol * K). Then, the calculated entropic term (TS) in the Gibbs free energy at 298.15 K was 0.40 eV for H_2 and 0.58 eV H_2O, respectively.[40, 41] Note that it is usually difficult to calculate the liquid-phase free energies with standard DFT methods. So we calculated liquid phase H_2O with a correction of 0.09 eV under 0.035 bars as the reference state since at this pressure gas phase H_2O is in equilibrium with liquid water at 298.15 K. Thus, the final entropic term of liquid water was 0.67 eV (0.58 + 0.09 = 0.67 eV). For the adsorbates, only vibrational entropy was taken into account to calculate the entropy corrections in the Gibbs free energy due to the negligible contributions of the translational and rotational entropies. Zero-point energies of the free molecules as well as the oxygenated intermediates were calculated from the DFT calculated vibrational frequencies. Especially, vibrational frequencies of adsorbed species were calculated by fixing catalyst substrate. Owing to the high-spin ground state of the O_2 molecule, it cannot be accurately described in DFT computations.[42, 43] Thus we calculated all free energies relative to H_2O(l) and H_2(g).

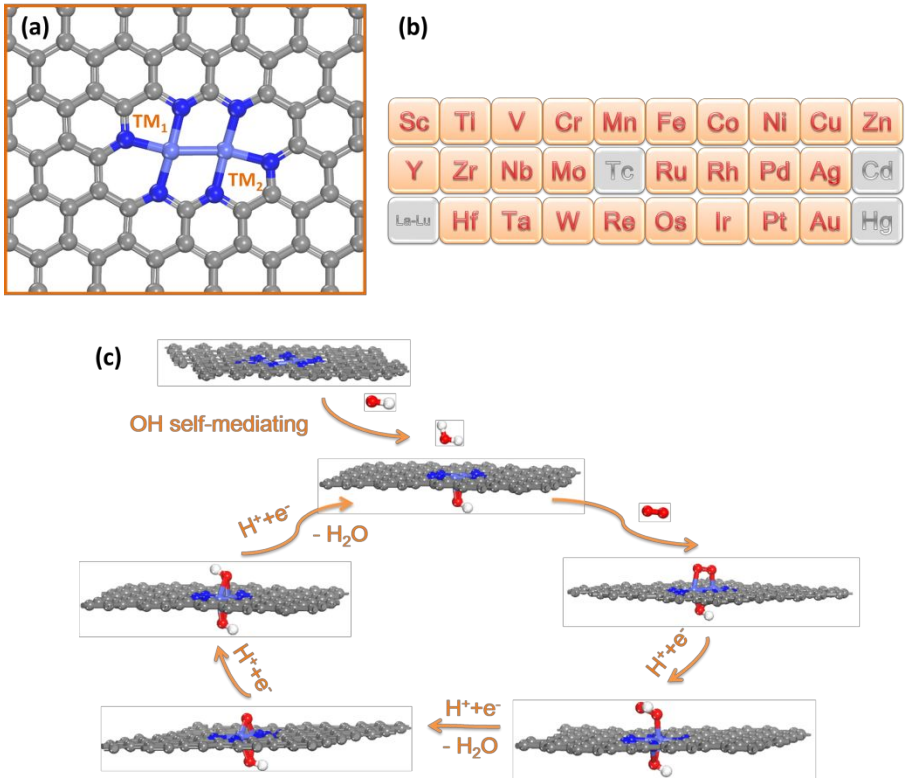

Figure 1. Geometric structure of BACs (a), the explored transition metal atom for metal dimer (b), and the OH species self-mediating mechanism on BACs (c).

Results and Discussion

Catalytic activity of homonuclear BACs.

In this work, all 3d, 4d, and 5d transition metals were selected to construct BACs, except for Tc, Cd, and Hg with the toxic/radioactive nature. Thus, 26 metal atoms were considered to construct BACs (Figure 1b). We will first focus on the activity of homonuclear BACs and then explore more complicated heteronuclear BACs. As revealed by Zelenay and coworkers,[44] the FeN_4 as the catalytic active site for ORR, which was directly visualized by aberration-corrected scanning transmission electron microscopy. Amazingly, a highly ORR activity can be achieved, when FeN_4 site spontaneously ligated by *OH in the fuel cell environment. In addition, some other

studies also indicated *OH species will boost ORR activity and binds on active sites strongly.[45-48] Based on this, a modifying sounds of *OH species was adopted as our BACs model to explore the ORR performance (Figure 1c). According to the previous studies, the oxygen molecule prefers to adsorb onto BACs via cis-bridged model, which plays an important role in the activation and weakening of O-O bond, precluding the possibility in the formation of H_2O_2 intermediate.[26] Therefore, we only considered the $4e^-$ mechanism to form H_2O. Typically, both associative and dissociative mechanisms are considered, depending on whether the O_2 molecule dissociates before reduction (detailed pathway seen in SR1-SR4 and SR5-SR9 in SI). Theoretically, the limiting potential (U_L) where all steps are downhill in free energy is usually used as a measure to evaluate the intrinsic activity and the corresponding U_L on Pt(111) ($U_L = 0.80$ V) was set as an benchmark for comparison. Accordingly, M2/NC with comparable or more positive U_L value compared to that of Pt(111) is considered as a promising ORR catalyst. In general, the direct O-O cleavage is unfavorable owing to the highly stable and strong O=O bond, thus we first investigated the associative mechanism. The adsorption free energy of oxygenated intermediates involved in associative mechanism and the corresponding limiting potential were summarized in Table S1. In addition, we also investigated the O_2 dissociation mechanism. It found that O_2 bonds strongly on early transition metal BACs (including Sc, Ti, V, Cr, Y, Zr, Nb, Mo, Ru, Hf, Ta, W and Re) and can dissociate into two separated O atoms; while for the late transition metal BACs, the O_2 dissociation is energetically very endothermic. Thus, we calculated the dissociative

mechanism on the above mentioned early transition metal BACs. The adsorption free energy of oxygenated intermediates involved in dissociative mechanism and the corresponding limiting potential were summarized in Table S2. The final U_L of these early transition metal BACs would adopt the more positive U_L with higher activity between the associative and dissociative mechanism. Figure 2a presents the U_L for 26 homonuclear M_2/NC BACs. One can clearly see that only Co_2/NC can co-balance the adsorption of different reaction intermediates and exhibit outstanding ORR activity comparable to the Pt(111) surface, with a favorable U_L of 0.82 V. Noteworthy, among all the investigated homonuclear BACs, the limiting potential of the elements with d orbitals that are less than half filled is negative, which indicates unappreciated catalyst of ORR. The poor activities are related to their too strong binding interactions with the ORR intermediates. The variation in adsorption free energy is determined by the electronic structure of the active center. As presented in Figure S1, with the increasing in the number of d electrons, the d-band center of metal dimer tends to become more negative. The higher (the lower) in energy the d band is relative to the highest occupied state (the Fermi energy), the stronger (the weaker) the interaction with the adsorbates. Therefore, the metal dimer with too little or too much d electron is not suitable for effective ORR catalyst.

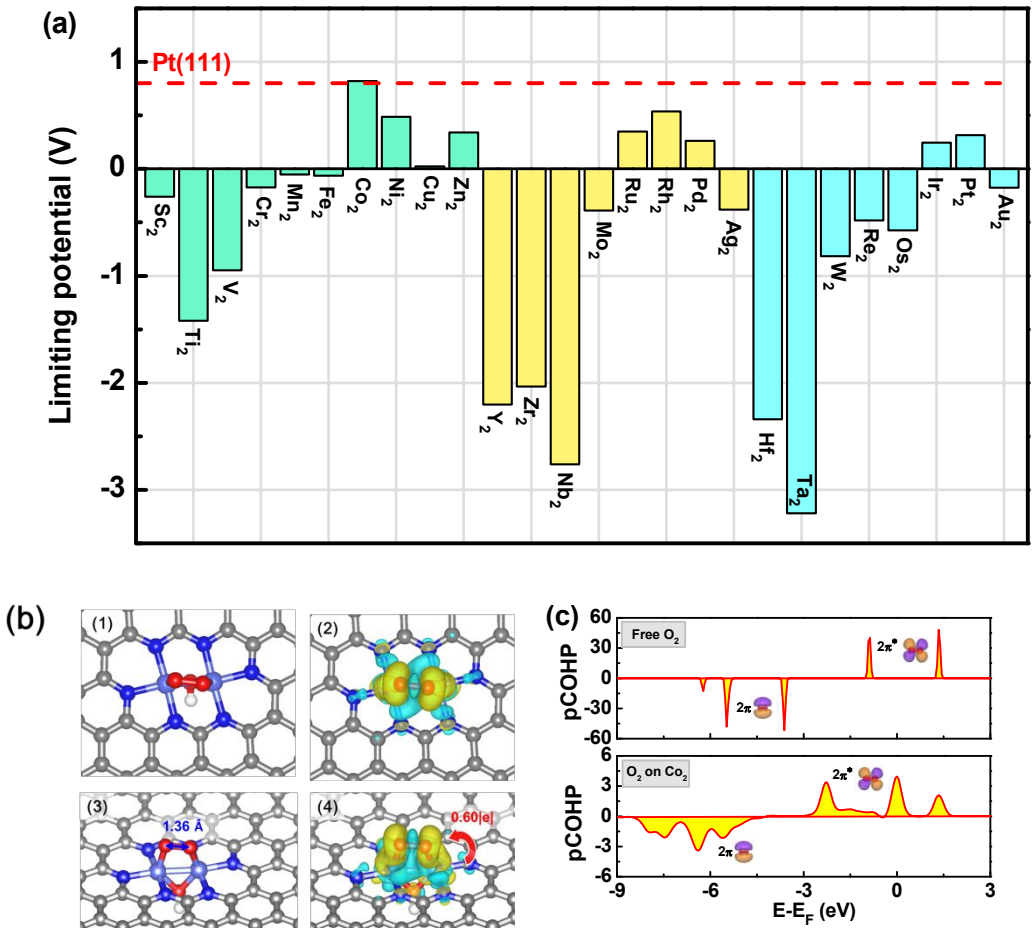

Figure 2. The ORR activity and electronic characterizations of homonuclear BACs. (a) Theoretical limiting potential (U_L) of 26 homonuclear M_2/NC BACs. (b) Optimized adsorption configuration and charge density difference of O_2 on Co_2/NC surface. (c) Projected crystal orbital Hamilton population (pCOHP) of free O_2 and adsorbed on Co_2/NC surface.

Why does Co_2/NC have a high activity towards ORR? To address this question, we carefully examined the adsorption and activation of O_2, a key step for ORR. Our computations demonstrated that O_2 is chemisorbed on Co_2/NC with a strong adsorption energy of -2.15 eV. As shown in Figure 2b, O_2 prefers to adsorb by coordination to two Co centers via cis-bridge configuration. Analyzing the charge

density difference revealed that the adsorbed O_2 interacts with Co_2/NC by the so-called "push-pull" mechanism, in which Co_2/NC would "push" electrons from the occupied *d* orbitals into the 2π* orbitals of O_2, and simultaneously "pull" the lone-pair electrons from the O_2 into the unoccupied *d* orbitals (Figure 2b). In this case, O_2 can be effectively activated with a remarkable O−O bond elongation to 1.36 Å from the gas phase value of 1.24 Å. Bader charge analysis indicated that about 0.60 electron is transferred from Co_2/NC to O_2. As a result, the 2π* orbitals of O_2 shift down in energy and become broadened and split as compared to the free O_2 molecule, as evidenced by the projected crystal orbital Hamilton population (pCOHP) analysis (Figure 2c).[49] The effective activation and weakening of the O-O bond is expected to facilitate the subsequent ORR steps, as confirmed by the calculated reaction free energies for each ORR elementary step based on the Co_2/NC catalyst (Figure S2). At the equilibrium potential of U = 1.23 V (pink line), the reduction of $*O_2$ to *OOH (the first reduction step) is the rate-determining step, with an uphill free energy of 0.41 eV. At the thermodynamic limiting potential (blue line) of 0.82 V, all the reaction steps are downhill in free energy. As far as the geometries of the adsorbed intermediates (*OOH, *O and *OH) are concerned, the *O and *OH are co-adsorbed by the two Co-Co atoms, while *OOH is only bonded to one of the Co atoms (for details, see Table S3).

Catalytic Activity of Heteronuclear BACs.

On the other hand, for most of the studied homonuclear BACs, a volcano-shaped relationship exists between the limiting potential and the adsorption free energy of

*OH species (ΔG_{*OH}) (Figure 3a). One can see that Co_2/NC, which exhibits the highest ORR activity among all the studied homonuclear candidates, is located close to the top of the volcano curve. Note that catalysts located on the left side have strong binding strength of *OH, and the activities are mainly limited by the step of *OH reduction to H_2O ($*OH + H^+ + e^- \leftrightarrow * + H_2O$), in comparison, those located on the right side exhibit weaker binding of *OH, and the ORR activities are limited by the step of $*O_2$ reduction to *OOH ($*O_2 + H^+ + e^- \leftrightarrow *OOH$). In principle, a viable ORR catalyst should have moderate adsorption to balance the binding for multiple ORR intermediates, and the limiting potential has to be as positive as possible to drive the occurrence of the reaction. From Figure 3a, about 11 homonuclear BACs are identified to locate around the top region of the volcano plot with limiting potential close to or above 0 V, including Fe, Mn, Ir, Ru, Rh, Co, Zn, Ni, Pt, Pd and Cu. Unfortunately, most of them (except for Co) are catalytically unsatisfactory due to the very low limiting potentials. This leaves a large room for activity tuning and improvement. Introducing heteronuclear centers by combining two different functional metal sites from either the left branch or right branch of the volcano plot would provide wider tunability and flexibility in modulating the adsorption strengths and ORR activities. Based on this hypothesis, we then extended our study to 55 heteronuclear BACs (M_1M_2/NC) by mixing the above screened 11 metal atoms with U_L close to or above 0 V.

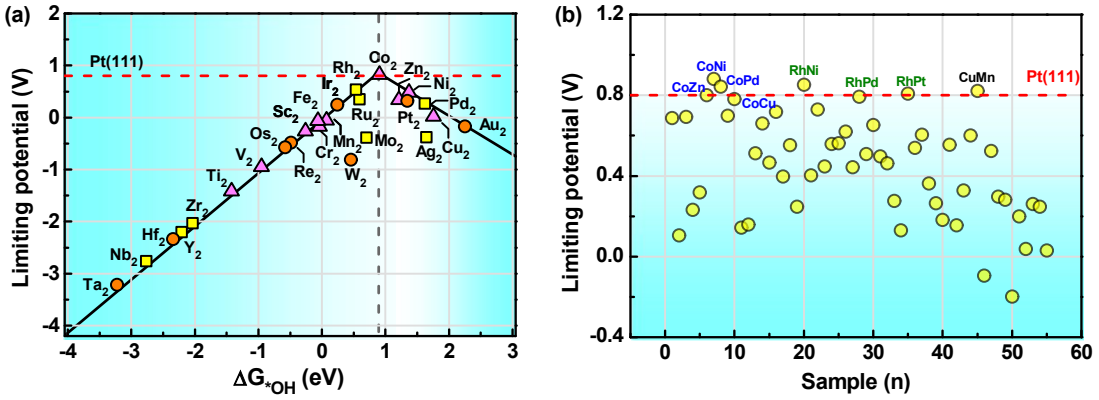

Figure 3. U_L of the homonuclear and heteronuclear BACs. (a) Volcano plot relationship between U_L and the adsorption free energy of *OH based on the homonuclear BACs. (b) The predicted U_L of the 55 heteronuclear BACs, only the promising candidates with comparable activity to the Pt(111) benchmark were shown with compositions.

Figure 3b summarizes the calculated U_L of the 55 heteronuclear BACs (the detailed adsorption strengths of ORR intermediates for each system are given in Table S4). Excitedly, 8 of 55 heteronuclear BACs stand out as highly promising candidates with activity comparable to the Pt(111) surface, including four Co-based BACs (CoZn/NC (0.80 V), CoNi/NC (0.88 V), CoPd/NC (0.84 V), CoCu/NC (0.78 V)), three Rh-based BACs (RhNi/NC (0.85 V), RhPd/NC (0.79 V), RhPt/NC (0.81 V)), and CuMn/NC (0.82 V). We should note that 3 heteronuclear BACs (CoNi, CoPd, and RhNi) display more positive U_L values than the homonuclear Co_2/NC counterpart (0.82 V), thus implying the intrinsically higher ORR activity. The optimal adsorption geometries of *OOH, *O, and *OH on the identified 8 BACs systems are depicted in Table S3. The *O species is usually co-adsorbed and bonded to the two metals. Due to the structural unsymmetry of the heteronuclear sites, the adsorption of

*OOH and *OH species becomes more complicated. Specifically, for the Co-based CoZn/NC, CoNi/NC and CoCu/NC systems, the active site to bind the *OOH and *OH intermediates occurs solely at the Co site. While for CoPd/NC, although *OOH and *OH prefer to be co-adsorbed by both the Co and Pd atoms, the intermediates are found to locate much closer to the Co center. Similarly, for the Rh-based BACs, except for RhNi/NC where *OOH is solely bonded to the Rh site, the *OH and *OOH prefer to be co-adsorbed by the Rh-Ni, Rh-Pd and Rh-Pt centers, but are geometrically located closer to the Rh site. These indicate that the introduction of the secondary metals can effectively tune the adsorption of ORR intermediates, yet the main active site for binding *OOH or *OH species still occurs at the Co or Rh site, which belongs to the same VIII group with nine outer electrons. In fact, if we take a closer look at the activities of the formerly investigated homonuclear BACs (Figure 2a), it can be observed that from groups 7 to 12 (such as Mn to Zn), with the increasing in the number of outer electrons, the limiting potential tends to firstly increase and then decrease. The increased valence electrons in the d-orbitals of the active metal site would partially occupy the M−O antibonding orbital, leading to the weakened adsorption of intermediates. Among them, Co or Rh is just at the right place, which can co-balance the adsorption strength of different intermediates and result in exceptional ORR activity. On the other hand, for the case of CuMn/NC catalyst, where Cu and Mn are located around two sides of Co, also facilitates ORR, and the active site for *OOH and *OH binding occurs solely at the Mn site (Table S3).

Then, we studied the free energy diagrams for O_2 reduction to H_2O on the eight heteronuclear BACs (Figure S3). At the equilibrium potential (1.23 V), the activities of the identified CoZn/NC, CoPd/NC, RhNi/NC, RhPt/NC and CuMn/NC candidates are determined by the reduction of *OH to H_2O ($* OH + H^+ + e^- \leftrightarrow * + H_2O$)), whereas the CoCu/NC and RhPd/NC catalysts are determined by the reduction from $*O_2$ to *OOH ($* O_2 + H^+ + e^- \leftrightarrow * OOH$). A particular case is found for the CoNi/NC catalyst, where the activity is determined by two reduction steps (from $*O_2$ to *OOH and from *OH to H_2O) having the same value of free energy increase (0.35 eV).

In a brief summary, our above analyses screened out one homonuclear and eight heteronuclear BACs with theoretical limiting potentials (between 0.78 V and 0.88 V) comparable and even superior to the Pt-based materials (~ 0.80 V), especially the most active BAC, namely CoNi/NC, has a limiting potential of 0.88 V.

In addition to the high activity, stability is another key criterion to evaluate an electrocatalyst, and only those catalysts with high structural stability can have great potential for synthesis. Thus, we evaluated the stabilities of the above screened BACs by calculating the formation energy (E_f), which is defined as $E_f = E(MM'@SUB) - E(SUB) - E(M) - E(M')$, where $E(MM'@SUB)$ and $E(SUB)$ are the total energies of BACs and substrate; $E(M)$ and $E(M')$ denote the total energies of the single metal atom in the bulk phase. According to this definition, when E_f is negative, the formation of bi-atom metal moieties is energetically favorable. As seen in Figure 4, E_f of all our screened BACs have negative formation energies, indicating that the

aggregation of metal atoms could be suppressed in thermodynamics. Furthermore, the stability of substrate has been evaluated by formation energy ($E_f^{'}$) as reference to graphene and nitrogen ($E_f^{'} = E(\mathrm{SUB}) - n\mu_C - m\mu_N$), where $E(\mathrm{SUB})$ represents the total energy of substrate, n and m denote the total number of C and N atoms, and μ_C and μ_N are the chemical potentials of C and N atoms, respectively. μ_C and μ_N are calculated from pristine graphene and nitrogen in gas phase. The $E_f^{'}$ of the substrate used in this work (pyriN6 in Table S5) is 3.99 eV, which is lower than that of the pyrroN3 substrate (Table S5). Noteworthy, the pyrroN3 has been successfully fabricated and characterized in experiment.[50] Finally, the $E_f^{'}$ of the nine promising BACs was also investigated as reference to graphene and nitrogen ($E_f^{'} = E(\mathrm{MM}^{'}@\mathrm{SUB}) - n\mu_C - m\mu_N - E(\mathrm{M}) - E(\mathrm{M}^{'})$. From Table S6, the $E_f^{'}$ of the nine BACs (2.2 ~ 3.3 eV) become lower compared with that of the substrate (3.99 eV), indicating that the nine dimers incorporate into the substrate will help to stabilize the system. These results manifested that our screened high-performance homonuclear and heteronuclear BACs exhibit high thermodynamic stabilities and hold strong potential for experimental realizations.

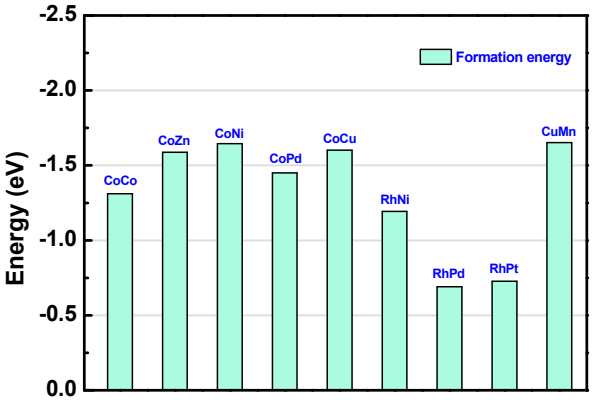

Figure 4. Formation energy of the nine promising BACs.

Noting that among the predicted bi-atomic pairs, two heteronuclear (CoNi/NC and CoZn/NC) and one homonuclear (CoCo/NC) BACs have been successfully synthesized by the recent experiments,[23-25] and they all demonstrated remarkable ORR performances. In the case of CoZn/NC electrocatalyst, the *in situ* XANES analysis in experiment also suggests Co as the major active center during the ORR,[25] which is in good agreement with our theoretical predictions. These experimental results strongly evidenced the predictive power of our computational investigation. With high stabilities and similar inherent ORR potentials, we strongly believe that the other yet unexplored BACs, such as CoCu, CoPd, RhPd, RhPt, RhNi and CuMn, can be realized experimentally in the very near future.

Origin of Activity.

It is generally accepted that the ORR activity is mainly determined by the adsorption free energy of *OOH, *O and *OH species. They tend to scale linearly with each other, leading to the formation of volcano-shaped activity, which is widely applied as a simple descriptor to describe the catalytic activity.[4, 51-53] The linear relationships between ΔG_{*OOH} *vs.* ΔG_{*OH} and ΔG_{*O} *vs.* ΔG_{*OH} are strongly correlated on the traditional transition metal surfaces.[53] However, in the case of the studied bi-atom catalysts, we found that their linear relationships are significantly weakened (Figure 5a and Figure 5b). This phenomenon can be understood by the significant difference between the intermediates adsorption over BACs and transition-metal surfaces. On

the transition-metal surfaces, *OOH (or *OH) prefers to adsorb to the atop sites, and *O normally adsorbs on the hollow sites. Whereas for BACs, there is no hollow sites available for *O adsorption, and O* tends to be shared by the two metal centers. Moreover, for *OOH or *OH, some of them prefer the bridge sites between two metal sites, while others prefer to bind only with one of the metal centers (as seen in Table S3), showing strong dependence on the heteronuclear bi-atom compositions. Due to these differences, BACs systems are much more complicated than the transition metal surface. Consequently, it is very difficult to precisely describe the ORR activity of BACs with only one descriptor.

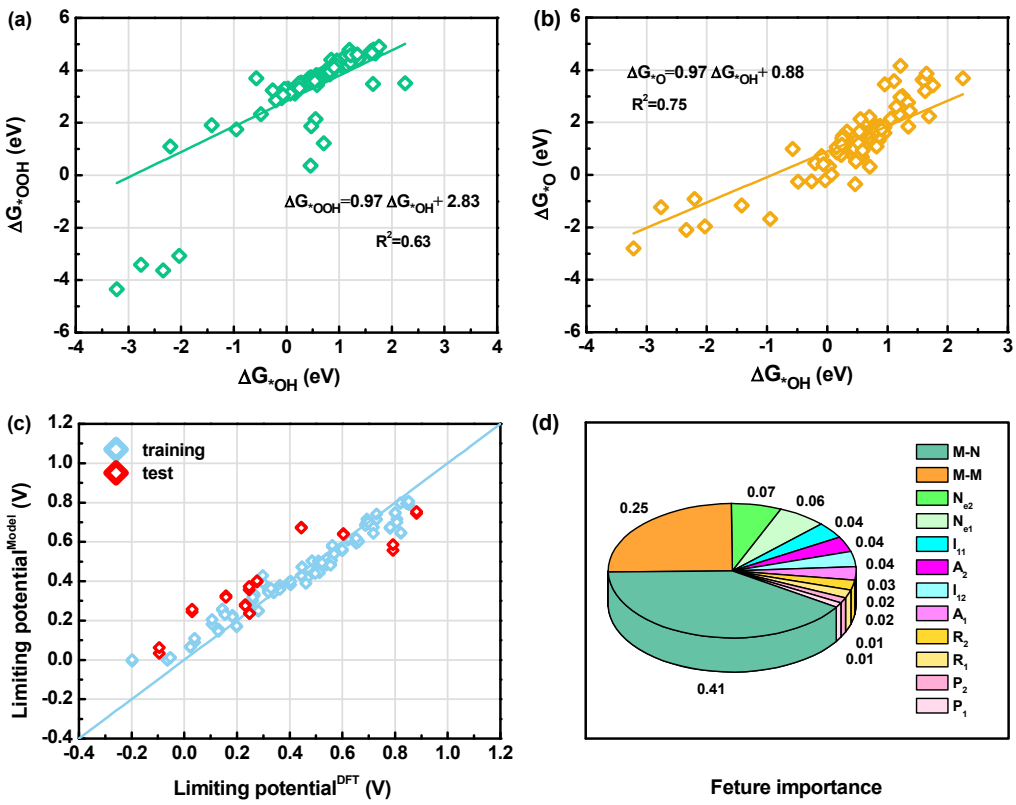

Figure 5. Linear relationships among the adsorption free energy obtained from DFT calculations (a and b) and results of machine-learning (c and d). (a) and (b): Linear relationships of ΔG_{*OOH}

vs. ΔG_{*OH} and ΔG_{*O} *vs.* ΔG_{*OH} on heteronuclear BACs. (c) Comparison of DFT-obtained U_L with those predicted values. (d) The feature importance based on the random forest regressor.

Thus, we employed the machine-learning method to explore the correlation between U_L and the intrinsic descriptor of the 11 homonuclear and 55 heteronuclear BACs catalysts. The success of machine-learning algorithm depends on the quality of the numerical descriptions of the studied systems. In our case, a feature set with seven descriptors was selected to describe the geometrical and electronic features of BACs, including the distance of two metal atoms (M-M), the average distance between two metal atoms and the coordinated N atoms (M-N), the Radii of two metal atoms (R_1 and R_2), the outer electron number of two metal atoms (N_{e1} and N_{e2}), the Pauling electronegativity (P_1 and P_2), the first ionization energy (I_1 and I_2) and the electron affinity (A_1 and A_2) of the two metals. Note that each heteronuclear dimer corresponds to two sets of BACs compositions (M_1M_2/NC and M_2M_1/NC), which actually denote the same BACs. Thus, we carried out a data enhancement for all the studied heteronuclear BACs, and in this way, each heteronuclear BAC has two sets of input features (Table S7).

We applied the random forest regressor in scikit learn toolkit,[54, 55] a family of machine learning algorithm, to explore the correlation between DFT-obtained limiting potential and the feature properties. The input data of U_L obtained from DFT calculations (Table S1 and Table S4) were randomly shuffled and divided into the training set and test set with a ratio of 5:1. As clearly shown in Figure 5c, our studied

model was trained effectively by the random forest regressor with a train score of 0.98 and a test score of 0.90 in Pearson correlation coefficient. Moreover, a lower mean square error for train set and test set of 0.004 and 0.022 was achieved, respectively. Furthermore, the importance of the selected seven features, which are closely related to the geometric and chemical properties affecting the catalytic performance, was also evaluated (Figure 5d). The feature of M-N and M-M distances are found to be the paramount factors in affecting the ORR activity of BACs with a feature importance of 0.41 and 0.25, respectively. Particularly, the delicate activity difference in the Co-based and Rh-based heteronuclear BACs can be rationalized to be a result of the geometry difference induced by the secondary metal. We should note that the outer electron number of metal atom (N_e) also plays an important role, although the influence becomes less prominent (with feature importance of 0.13). This can be understood by the formation of metal-metal bond between two metal atoms and those electrons cannot significantly help for binding ORR intermediates. Especially, the Co center and Rh center with suitable outer electrons tend to exhibit a high activity, while the other four descriptors have a relatively low feature importance. In addition, the M-M distance in homonuclear BACs and the corresponding values in bulk metals have been summarized in Table S8. One can see that among the investigated homonuclear BACs, the M-M distance is shorter than that in the bulk phase except for Co. This helps to explain and understand the difference in the ORR performance of BACs, and machine-learning method is a powerful tool to establish the intrinsic structure-property correlation.

Conclusion

The BACs have recently emerged as a new frontier in electrocatalysis. In this work, we explored the potential of atomically dispersed bi-atom catalysts (BACs) for ORR by means of systematic and comprehensive DFT computations coupled with machine-learning techniques. We first sampled 26 homonuclear (M_2/NC) BACs covering 26 transitional metal atoms, and then constructed 55 heteronuclear BACs based on the activity volcano curve of the homonuclear catalysts. Our screening process identified that one homonuclear (Co_2/NC) BAC and eight heteronuclear BACs (CoZn/NC, CoNi/NC, CoPd/NC, CoCu/NC, RhNi/NC, RhPd/NC, RhPt/NC, and CuMn/NC) are highly promising alternatives to the Pt-based catalysts. Among them, CoNi/NC possesses the most optimal activity with a very high limiting potential of 0.88 V. Furthermore, aided by the machine-learning method, we revealed the key factors that govern the ORR activity of BACs. The results indicated that ORR activity of BACs is mainly governed by simple geometry parameters (e.g., the distance of two metal atoms as well as the average distance between two metal atoms and the coordinated N atoms) and the physical properties of the metal atoms (e.g., outer electron number). Motivated by the recent experimental progress in fabricating BACs, our identified promising BACs hold great potential for future synthesis in experiment. This work not only identified highly promising BACs to replace the precious Pt catalysts but also provided useful insights for the design of high-performance electrocatalysts for ORR and other related electrochemical reactions.

Conflicts of interest

Dr. Chaofang Deng and Dr. Yang Su contributed equally to this work. The authors declare no competing financial interests.

Acknowledgements

This work is supported in China by the Science and Technology Research Program of Chongqing Municipal Education Commission (Grant NO. KJQN201801608), the Program of Innovation Center for Lipid Resource Utilization at Chongqing University of Education (No. 2017XJPT01), the Program for Innovative Research Team in Chongqing University of Education (No. CQYC201903178), the National Natural Science Foundation of China (No.21903008), the Chongqing Municipal Resources and Society Security Bureau (cx2019141), the Chongqing Science and Technology Commission (cstc2020jcyjmsxmX0382), and the Fundamental Research Funds for the Central Universities (2020CDJQY-A031, 2020CDJ-LHZZ-063), and in USA by the NSF Centre for the Advancement of Wearable Technologies (Grant 1849243). This research used resources of the National Supercomputer Center in Guangzhou.

Supporting Information

The Supplementary Materials include the computational details, adsorption free energy, limiting potential, formation energy and the adsorption geometry of ORR intermediates and input features of machine-learning.

References

(1) B. C. H. Steele; A. Heinzel, *Nature*, **2001**, *414* (*6861*)**,** 345-352.
(2) M. Winter; R. J. Brodd, *Chem. Rev.*, **2004**, *104* (*10*)**,** 4245-4270.
(3) A. A. Gewirth; J. A. Varnell, A. M. DiAscro, *Chem. Rev.*, **2018**, *118* (*5*)**,** 2313-2339.
(4) A. Kulkarni; S. Siahrostami; A. Patel, J. K. Nørskov, *Chem. Rev.*, **2018**, *118* (*5*)**,** 2302-2312.
(5) P. C. K. Vesborg, T. F. Jaramillo, *RSC Adv.*, **2012**, *2* (*21*)**,** 7933-7947.
(6) Y. Wang; Y. Li, T. Heine, *J. Am. Chem. Soc.*, **2018**, *140* (*40*)**,** 12732-12735.
(7) Z. Lu; G. Xu; C. He; T. Wang; L. Yang; Z. Yang, D. Ma, *Carbon*, **2015**, *84*500-508.
(8) C. Deng; F. Li, Q. Tang, *J. Phys. Chem. C*, **2019**, *123* (*44*)**,** 27116-27123.
(9) L.-y. Feng; Y.-j. Liu, J.-x. Zhao, *J. Power Sources*, **2015**, *287*431-438.
(10) Y. Wang; Y.-J. Tang, K. Zhou, *J. Am. Chem. Soc.*, **2019**, *141* (*36*)**,** 14115-14119.
(11) V. R. Stamenkovic; B. S. Mun; M. Arenz; K. J. J. Mayrhofer; C. A. Lucas; G. Wang; P. N. Ross, N. M. Markovic, *Nat. Mater.*, **2007**, *6*241-247.
(12) C. Wang; N. M. Markovic, V. R. Stamenkovic, *ACS Catal.*, **2012**, *2* (*5*)**,** 891-898.
(13) Z. Duan, G. Wang, *Phys. Chem. Chem. Phys.*, **2011**, *13* (*45*)**,** 20178-20187.
(14) H. A. Hansen; J. Rossmeisl, J. K. Nørskov, *Phys. Chem. Chem. Phys.*, **2008**, *10* (*25*)**,** 3722-3730.
(15) H. Zhang; G. Liu; L. Shi, J. Ye, *Adv. Energy Mater.*, **2018**, *8* (*1*)**,** 1701341.
(16) X.-F. Yang; A. Wang; B. Qiao; J. Li; J. Liu, T. Zhang, *Acc. Chem. Res.*, **2013**, *46* (*8*)**,** 1740-1748.
(17) Y. Wang; J. Mao; X. Meng; L. Yu; D. Deng, X. Bao, *Chem. Rev.*, **2019**, *119* (*3*)**,** 1806-1854.
(18) S. Ding; M. J. Hulsey; J. Perez-Ramirez, N. Yang, *Joule*, **2019**, *3* (*12*)**,** 2897-2929.
(19) Y. Pan; C. Zhang; Z. Liu; C. Chen, Y. Li, *Matter*, **2020**, *2* (*1*)**,** 78-110.
(20) Z. Li; S. Ji; Y. Liu; X. Cao; S. Tian; Y. Chen; Z. Niu, Y. Li, *Chem. Rev.*, **2020**, *120* (*2*)**,** 623-682.
(21) C. Wan; X. Duan, Y. Huang, *Adv. Energy Mater.*, **2020**, *10* (*14*), 1903815.
(22) J. Wang; W. Liu; G. Luo; Z. Li; C. Zhao; H. Zhang; M. Zhu; Q. Xu; X. Wang; C. Zhao; Y. Qu; Z. Yang; T. Yao; Y. Li; Y. Lin; Y. Wu, Y. Li, *Energ. Environ. Sci.*, **2018**, *11* (*12*)**,** 3375-3379.
(23) M. Xiao; H. Zhang; Y. Chen; J. Zhu; L. Gao; Z. Jin; J. Ge; Z. Jiang; S. Chen; C. Liu, W. Xing, *Nano Energy*, **2018**, *46*396-403.
(24) X. Han; X. Ling; D. Yu; D. Xie; L. Li; S. Peng; C. Zhong; N. Zhao; Y. Deng, W. Hu, *Adv. Mater.*, **2019**, *31* (*49*)**,** 1905622.
(25) Z. Lu; B. Wang; Y. Hu; W. Liu; Y. Zhao; R. Yang; Z. Li; J. Luo; B. Chi; Z. Jiang; M. Li; S. Mu; S. Liao; J. Zhang, X. Sun, *Angewandte Chemie*, **2019**, *131* (*9*)**,** 2648-2652.
(26) M. Xiao; Y. Chen; J. Zhu; H. Zhang; X. Zhao; L. Gao; X. Wang; J. Zhao; J. Ge; Z. Jiang; S. Chen; C. Liu, W. Xing, *J. Am. Chem. Soc.*, **2019**, *141* (*44*)**,** 17763-17770.
(27) X. Y. Guo; J. X. Gu; S. R. Lin; S. L. Zhang; Z. F. Chen, S. P. Huang, *J. Am. Chem. Soc.*, **2020**, *142* (*12*)**,** 5709-5721.
(28) F. Li; X. Liu, Z. Chen, *Small Methods*, **2019**, *3*1800480.
(29) J. Zhao; J. Zhao; F. Li, Z. Chen, *J. Phys. Chem. C*, **2018**, *122* (*34*)**,** 19712-19721.
(30) F. Li, Z. Chen, *Nanoscale*, **2018**, *10* (*33*)**,** 15696-15705.
(31) G. Kresse, J. Furthmüller, *Phys. Rev. B*, **1996**, *54* (*16*)**,** 11169-11186.
(32) J. P. Perdew; K. Burke, M. Ernzerhof, *Phys. Rev. Lett.*, **1996**, *77* (*18*)**,** 3865-3868.
(33) P. E. Blöchl, *Phys. Rev. B*, **1994**, *50* (*24*)**,** 17953-17979.

(34) S. Grimme; J. Antony; S. Ehrlich, H. Krieg, *J. Chem. Phys.*, **2010**, *132* (*15*)**,** 19.
(35) M. Fishman; H. L. L. Zhuang; K. Mathew; W. Dirschka, R. G. Hennig, *Phys. Rev. B*, **2013**, *87* (*24*)**,** 245402.
(36) K. Mathew; R. Sundararaman; K. Letchworth-Weaver; T. A. Arias, R. G. Hennig, *J. Chem. Phys.*, **2014**, *140* (*8*)**,** 084106.
(37) H. Johll; H. C. Kang, E. S. Tok, *Phys. Rev. B*, **2009**, *79* (*24*)**,** 18.
(38) J. K. Nørskov; J. Rossmeisl; A. Logadottir; L. Lindqvist; J. R. Kitchin; T. Bligaard, H. Jónsson, *J. Phys. Chem. B*, **2004**, *108* (*46*)**,** 17886-17892.
(39) J. Rossmeisl; A. Logadottir, J. K. Norskov, *Chem. Phys.*, **2005**, *319* (*1-3*)**,** 178-184.
(40) X. Zhang; K. A. Min; W. Zheng; J. Hwang; B. Han, L. Y. S. Lee, *Appl. Catal. B-Environ.*, **2020**, *273,* 118927
(41) K. Nam; H. Chun; J. Hwang; K.-A. Min, B. Han, *ACS Sustainable Chem. Eng.*, **2020**, *8* (*29*)**,** 10852-10858.
(42) R. O. Jones, O. Gunnarsson, *Rev. Mod. Phys.*, **1989**, *61* (*3*)**,** 689-746.
(43) S. Kurth; J. P. Perdew, P. Blaha, *Int. J. Quantum Chem.*, **1999**, *75* (*4-5*)**,** 889-909.
(44) H. T. Chung; D. A. Cullen; D. Higgins; B. T. Sneed; E. F. Holby; K. L. More, P. Zelenay, *Science*, **2017**, *357* (*6350*)**,** 479-483.
(45) A. Zitolo; V. Goellner; V. Armel; M.-T. Sougrati; T. Mineva; L. Stievano; E. Fonda, F. Jaouen, *Nature Materials*, **2015**, *14* (*9*)**,** 937-942.
(46) Y. H. Zhao; J. X. Gu, Z. F. Chen, *Adv. Funct. Mater.*, **2019**, *29* (*44*)**,** 1904782.
(47) E. F. Holby, C. D. Taylor, *Sci Rep*, **2015**, 59286.
(48) J. Wang; Z. Q. Huang; W. Liu; C. R. Chang; H. L. Tang; Z. J. Li; W. X. Chen; C. J. Jia; T. Yao; S. Q. Wei; Y. Wu, Y. D. Lie, *J. Am. Chem. Soc.*, **2017**, *139* (*48*)**,** 17281-17284.
(49) S. Maintz; V. L. Deringer; A. L. Tchougreeff, R. Dronskowski, *J. Comput. Chem.*, **2016**, *37* (*11*)**,** 1030-1035.
(50) D. C. Wei; Y. Q. Liu; Y. Wang; H. L. Zhang; L. P. Huang, G. Yu, *Nano Lett.*, **2009**, *9* (*5*)**,** 1752-1758.
(51) N. Govindarajan; M. T. M. Koper; E. J. Meijer, F. Calle-Vallejo, *ACS Catal.*, **2019**, *9* (*5*)**,** 4218-4225.
(52) M. Anand, J. K. Nørskov, *ACS Catal.*, **2020**, *10* (*1*)**,** 336-345.
(53) V. Viswanathan; H. A. Hansen; J. Rossmeisl, J. K. Nørskov, *ACS Catal.*, **2012**, *2* (*8*)**,** 1654-1660.
(54) L. Breiman, *Mach. Learning*, **2001**, *45* (*1*)**,** 5-32.
(55) O. Kramer, Scikit-learn, Machine Learning for Evolution Strategies, Springer2016, pp. 45-53.